國立交通大學

光電工程學系

光電工程研究所

碩士論文

利用噴墨技術製造導光板微透鏡結構

Applications of Microlens Array by Ink-Jet Technology for LCD Backlight System

研究生：余宗翰

指導教授：田仲豪 博士

中華民國九十七年十月

利用噴墨技術製造導光板微透鏡結構

Applications of Microlens Array by Ink-Jet Technology for LCD Backlight System

研究生: 余宗翰　　Student: Tsung-Han Yu

指導教授: 田仲豪 博士　　Advisor: Dr. Chung-Hao Tien

國立交通大學 電機學院

光電工程學系

光電工程研究所

碩士論文

A Thesis

Submitted to Display Institute & Photonic Department

College of Electrical Engineering Science

National Chiao-Tung University

in Partial Fulfillment of the Requirements

for the Degree of Master

In

Institute of Electro-Optical Engineering

October 2008

Hsin-Chu, Taiwan, Republic of China

中華民國九十七年十月

利用噴墨技術製造導光板微透鏡結構

學生：余宗翰

指導教授：田仲豪 博士

國立交通大學

論文大綱

現今的導光板製造方式可分為印刷與非印刷製程技術，本研究應用噴墨製造技術來取代傳統製程技術，利用此技術來製作導光板下側所散布的微透鏡陣列結構，以達到降低成本與增加效率的生產優勢，本研究將針對十六比九，七吋導光板元件上做設計與製造。此導光結構能夠控制微透鏡曲率以及密度，驗證 82%的均勻性與 2477 nits 的正向亮度。除此之外，ink-jet 噴墨製程比起傳統列印技術，能夠節省超過 50%的材料消耗，並保持其光學特性。

Applications of Microlens Array by Ink-Jet Technology for LCD Backlight System

Student: Tsung-Han Yu

Advisor: Dr. Chung-Hao Tien

National Chiao Tung University

Abstract

This research describes a simple and cost effective method to fabricate a UV-curable epoxy microlens array with controlled curvature and filling factor, by which we implemented a 7-inch 16:9 format light guide plate with 82% uniformity and 2477 nits of brightness. Compared with the conventional dot printing technology, ink-jet printing is able to save 50% material consumption without sacrifice of any optical performance. Proposed method has a promising impact in microstructure fabrication with other polymer materials due to its simplicity and versatility.

誌謝

本論文得以順利完成，本人由衷的感謝指導教授田仲豪教授這二年多來的指導與提攜。老師平時教學態度認真嚴謹，對學生總不厭其煩的細心指導與諄諄教誨，使我能夠發揮潛力與才能，順利完成迎面而來的各項挑戰，並從中獲得許多寶貴的經驗與豐碩的果實，在此向田老師致上我最高的敬意與感恩。

在實驗室的日子裡，特別要感謝博士班的洪健翔學長，陸彥行學長，簡銘進學長和顯示系統實驗室的鄭榮安學長在研究方向以及實驗上的建議與討論，以及學弟蕭毅豪和林宗瑋，在實驗上面的合作與協助，讓我受益良多獲益匪淺。此外，也感謝鄭壁如學姐，藍子翔學長以及已經畢業的學長們在研究過程中提供許多寶貴的經驗與建議。當然，這兩年在實驗室一起度過的同學:　蕭人彰，潘紀豪，鍾積賢，洪瑋琮及呂柏毅，謝謝你們讓我在這段研究的生活更加充實與快樂，以及學弟妹在課業上，生活上與研究上的幫助與分享，並陪伴我一起度過這的日子。

此外，我要感謝優貝克的林郁欣先生和中華映管的李宗陽先生，在研究期間提供我實驗及技術上的重要協助，讓我實驗得以順利完成。

最後，對於我最愛的家人以及許多朋友，我要感謝你們多年來的支持與鼓勵，還有生活上的細心照顧與關懷，使我能夠無後顧之憂的研究與學習，並順利完成碩士學業。總之，要感謝的人太多了，最後也謝謝我自己。

Tsung Han Yu

Table of Contents

Figure Captions

Table of Contents

Chapter 1

Introduction

1.1 Overview

Since the twentieth century, display technology has been rapidly advancing. With the popularization of computer and internet, display devices and enormous information interchange become parts of our live, besides, the demand of technologies of displaying mass information in pictures and contents are necessary.

Electronic displays are key component to facilitate information presentations. As an interface between human being and information devices, electronic displays are demanded to process sufficient information content and be operated in various applications with different criteria, such as high resolution, high contrast ratio, high brightness, high readability, wide viewing angle, fast response time, portability, and high tolerance of environment variations. In order to satisfy the different demands, diverse display technologies have been demonstrated in the past years.

CRTs techniques have developed maturely, most of researcher are continuously making breakthroughs to introduce flat panel, such as liquid crystal displays (LCDs), electroluminescent (EL) displays, plasma display panels (PDPs), and light emitting diode (LED) displays.[1]

Up to now, LCD is the most successful display, which has the desired features of thin format, light weight, low power consumption, and high image quality at the same time. All these properties can fulfill the requirements of the applications including mobile phones, PDA (personal digital assistant), notebook, portable information apparatuses, digital camera, etc.

With the developments of these various applications, LCDs have become the most important information displays as the role of CRTs in the twentieth century.

1.1.1 Liquid Crystal Displays

Liquid crystal (LC) does not emit light but plays a role of an electro-optical shutter to modulate the transmission of incident light in the LCD structure. Thus, a backlight system is adopted and placed behind the display to provide the emissive light for the LCD.[2,3]

A configuration of the LCD is shown in Fig. 1-1.[4] LC material is placed between two glass substrates, where the indium tin oxide (ITO) electrode is coated. Therefore, the twist angle of LC can be controlled by the applied voltage, and then the amount of transmitted light can be modulated.[5] Besides, the RGB color filters on the upper glass substrate mix the three monochromatic primary colors to produce the full color images.

LCDs have many advantages, such as high definition, light weight, small thickness, and less radiation. Due to these benefits, LCDs become the most widespread technology among the whole flat panel displays (FPDs). However, with the increasing of size, the uniformity, brightness, and power-saving become serious issues, which needed to be resolved. Therefore, the optimization of backlight system is an important work.

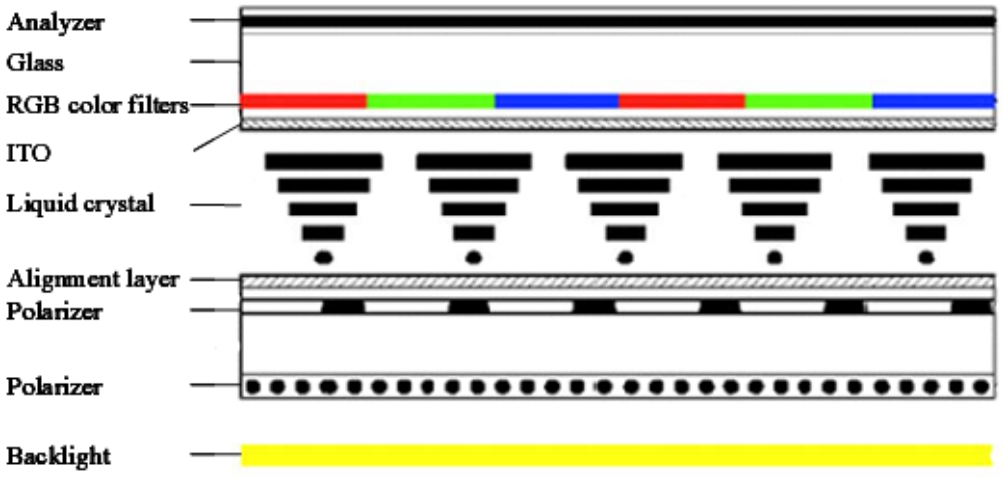

Fig. 1-1 A cross section view of LCD

1.2 Backlight Module

1.2.1 Division of Backlight Module by Different Light Source Position

The backlight module can be roughly classified two types: side-emitting type and directly-view type as shown in Fig. 1-2. Side-emitting backlight system is usually applied in small size products, such as laptop and mobile phone. Directly-emitting backlight system is abundantly used in large size products, such as monitor and TV.

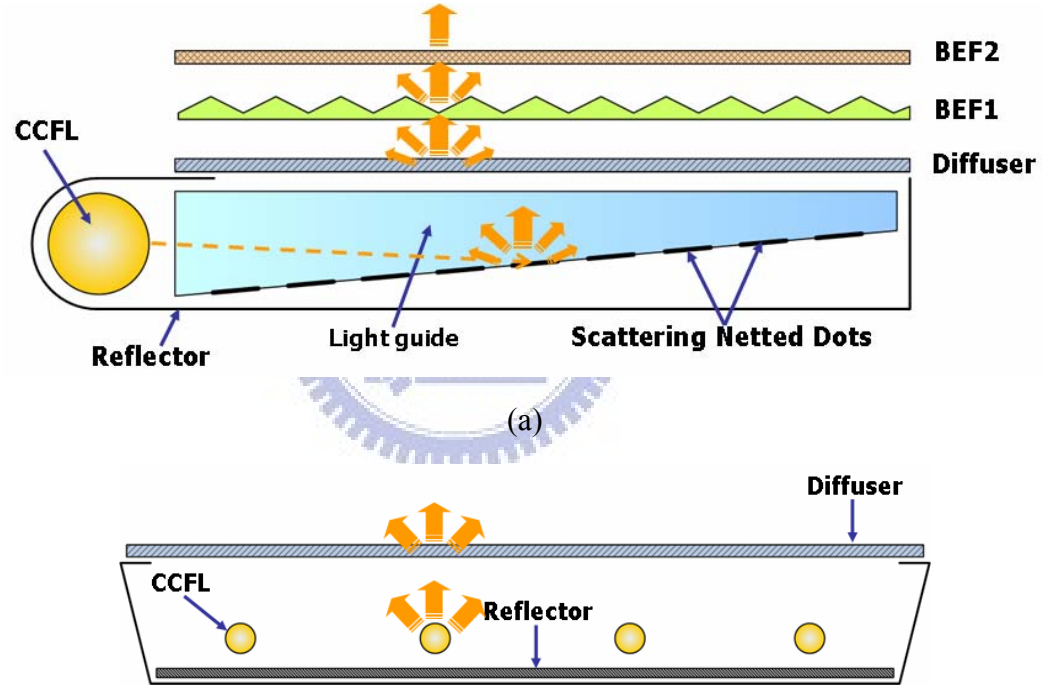

Fig. 1-2 The schematic of different type of backlight system (a) directlit type (b) sidelit type

1.2.2 Main Parts of Backlight Module

In view of the preceding introduction, several parts of backlight modulate are as following:

- Light guide plate (LGP):

The LGP guides the direction of the light in order to improve brightness and uniformity. Therefore, the LGP is an important key component for backlight module. Generally, the light-guiding plate (LGP) can be fabricated in terms of printing molding or non-printing molding. In printing molding, diffusing dots are printed through the screen printing on the bottom of LGP by using a material with high transmittance. However, the light distribution is hard to control due to the scattering effect. In non-printing molding, the slot-cut or injection molding is usually used to fabricate the micro structures on the LGP, and the brightness and directivity can be improved by such micro structures. There are several manufacturing methods shown in Table 1-1 .

Table 1-1 Comparison of manufacturing methods

Method	Features	Pros/Cons
Screen printing	The diffusing dots are printed through the screen printing on the bottom of LGP by using high transmission paint.（SiO_2 or TiO_2）	Fast, low cost. The brightness and uniformity are adequate. Short life time.
Injection molding	The diffusing dots are printed through the injection printing.（40~50um)	Standard manufacturing process. Molding-process is expensive.
Slot-cut	The diamond knife is usually used to incise the v-cut groove structures.	High brightness and accuracy. Material-wasting, time-consuming, and expensive.

- Light source:

Basically, the light source can be divided into LED and CCFL. LED has been used more

commonly as the light source for backlight module in small size. However, CCFL is still the main light source for large size LCD. LED has improved and the effectiveness is nearly as good as traditional CCFL, and with only more advantages. LED backlighting can increase the brightness, low power consumption, and fast response time.

- Reflector:

The reflector can wrap the CCFL tube to avoid light linkage and improve the reflecting efficiency.

- Diffusive sheet and prism sheet:

When light is emitted from the light source, it is diffused by the diffusive plate and reflected by the reflector. A bottom diffusive sheet with adjusted scattering ability is applied to get better uniform light distribution. After that, a prism sheet, so-called brightness enhancement film (BEF), is used to redirect the light from the inclined angle to the normal direction, and thus enhancing brightness in the normal direction. Finally, a top diffusive sheet is applied to protect the micro-structure of the prism and uniform the light.

1.3 Motivation and Objective

A light guide plate (LGP) is an essential component to implement a uniform planar source for liquid crystal display (LCD). As shown in Fig. 1-3, the conventional design has a specific pattern of diffusing white spots on the bottom surface, where the diffusing dot pattern serves to spread the incident light from sources over a wide angle to keep the luminance uniform over the entire display area. Many approaches were developed to replace the typical diffusing white dots with designed microfeatures and the corresponding fabrication process. Compared with conventional opal-coated and sandblasted diffusers subject to Lambertian or Gaussian radiation patterns, microlens arrays (MLAs) are one of the most promising approaches for customized tailoring of the characteristics of scattering behavior.

By controlling the microlens profile and arrangement of the MLA, the angular distribution and extracting efficiency of the LGP can be adjusted accordingly. However, it is not easy to in-situ modulate the profile and arrangement by the bench process such as photoresist reflow, micromolding, mass transport, direct lithography. Instead, several rising technologies like laser engraving or ink-jet technology would be advantageous to form the relatively complex optical microstructure in a flexible process. Ink-jet printing is a non-contact dot-matrix printing technology in which droplets of ink are jetted from a small aperture directly to a specified position on a substrate to create microfeatures. In this paper, we developed a novel high-precision multi-head, multi-nozzle inkjet printer that utilizes graphical printing to implement a 7-inch 16:9 format light guide plate for LCD application.

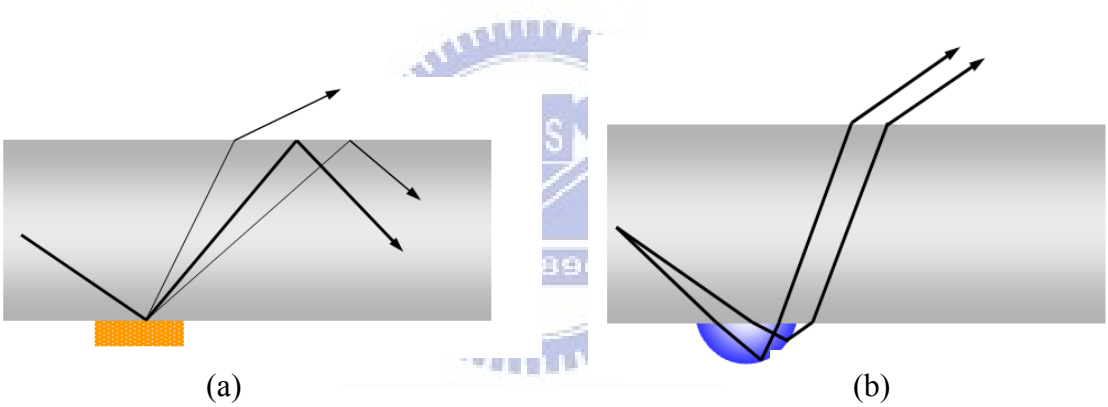

Fig. 1-3 The optical properties of (a) conventional diffusing pattern and (b) microlens deflector

1.4 Organization of this thesis

This thesis is organized as following: The basic knowledge of inkjet printing and optical principles are described in **Chapter 2.** The experimental details are presented in **Chapter 3**, and the droplets analysis related to formation is also illustrated. In **Chapter 4**, the experimental results and optical measurement are investigated. The performance of LGP by ink-jet printing is also demonstrated and summarized. Finally, the conclusions and future work will be given in **Chapter 5**.

Chapter 2

Introduction of the Ink-jet Printing System and Optical Principles

The principle of ink-jet printing system will be introduced. Besides, the physical phenomena associated with the droplets formed by ink-jet printing will be presented.

2.1 Ink-jet Printing System

Ink-jet printers can operate either in continuous or drop-on-demand (DOD) mode.[6] In continuous mode Fig. 2-1(a), the ink is pumped through a nozzle to form a liquid jet. Uniformly space and sized droplets are obtained by imposing a perturbation, leading to a surface-tension driven jet ink break-up. Generally, continuous-mode is mainly used for high-speed graphical applications such as textile printing and labeling. In DOD mode Fig. 2-1 (b), an acoustic pulse ejects ink droplets to form a reservoir through a nozzle. In comparison, the DOD mode is more suitable for electronic industries based on its smaller droplet size and higher placement accuracy.

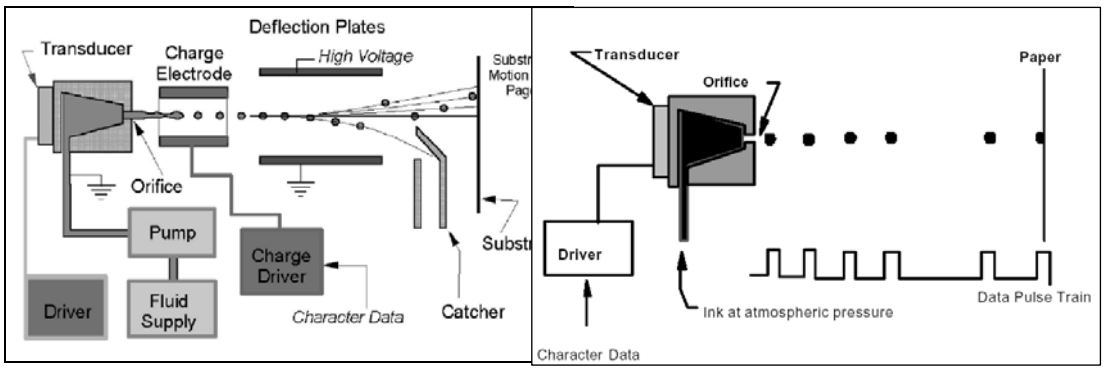

(a) (b)

Fig. 2-1 Inkjet printing system

2.1.1 Drop-on-demand Mode

In the DOD mode, the acoustic pulse can be generated either thermally or piezoelectrically. In thermal DOD ejection, solvent is heated to vaporize and a rapidly expanding vapor bubble is created so that an ink droplet is ejected, as shown in Fig. 2-2 (a). The main problem of thermal DOD is that ink always has a lot of restrictions because the ink for industrial application is always temperature sensitive. On the other hand, in piezoelectric DOD mode, ink is expelled by the deformation of a piezoelectric crystal when an electric potential is applied, as shown in Fig. 2-2(b). Piezoelectric DOD is more suitable for a verity of inks because ink degradation is no longer a concern since the pressure wave is generated strictly through mechanical deformation.

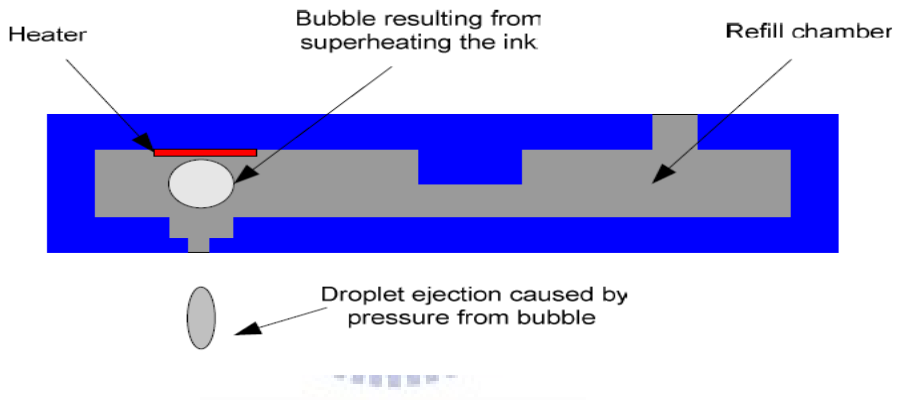

(a)

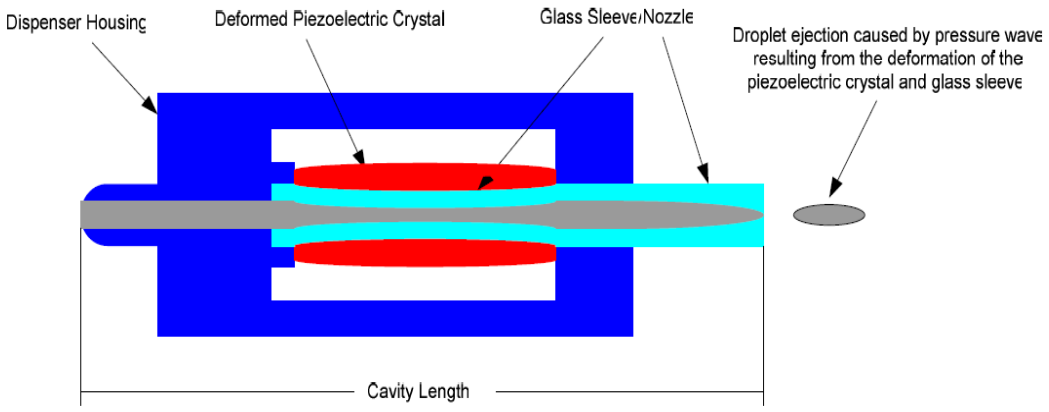

(b)

Fig. 2-2 (a) A typical bubble jet dispenser and (b) a typical piezoelectric jet dispenser.

There are numerous companies producing inkjet printers for industrial printing purposes. Because of using a single nozzle is not realistic in industrial applications, and multi-nozzle inkjet printing heads have been invented. The Platform from microdrop was built around eight glass nozzles running in parallel. The 80L and 140P Piezo Micro Deposition System which are develop by Litrex, equip with several hundred of individual nozzles for manufacturing PLED displays.

2.1.2 Precision of Ink-jet Printer

A challenge for ink-jet printing system is the precision. The position of a printed drop is affected by several parameters during ejecting process. For instance, an analysis of printed conductive polymers showed that droplet position can vary by approximately ±11 μm. In the case of digital lithography, the ejected droplet is positioned along the printing direction by translation of the print head, defined as the *x* direction. The relative position of a droplet with respect to the position of the print head when the ejection signal is applied is given by the equation:

$$x \approx \frac{us}{v\cos\theta} + ut + s\tan\theta \quad (2\text{-}1)$$

Where *u* is the print head translation velocity, u is the drop ejection velocity, *s* is the distance between the drop and the print head, θ is the angle of the drop from the normal direction, and *t* is the time that the droplet ejects from the head after the signal was applied, as shown in Fig. 2-3.

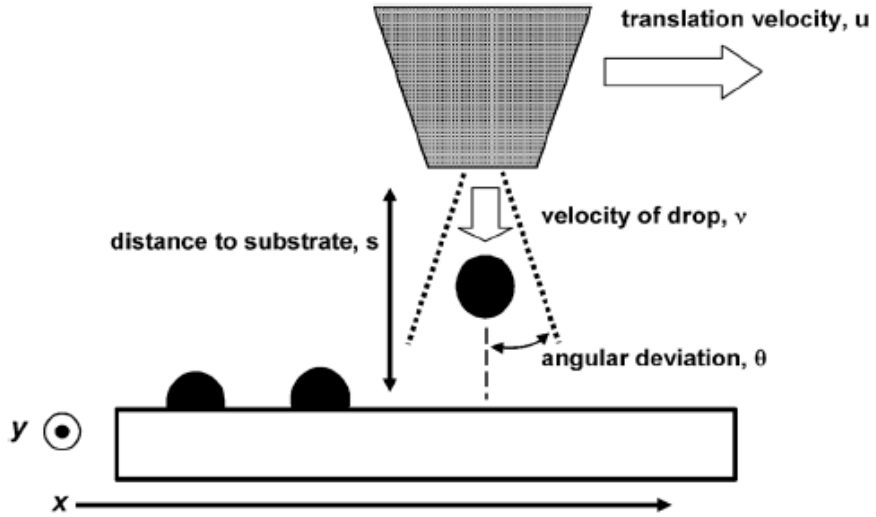

Fig. 2-3 Schematic representation of droplet ejection for inkjet printing.

The error in printing for the *x* direction can be approximated by taking the differential of Eq. 2-1 and is given as following:

$$\Delta x \approx \frac{us}{v\cos\theta}\left(\frac{\Delta u}{u}+\frac{\Delta s}{s}+\frac{\Delta v}{v}\right)+s\sec\theta\cdot\Delta\theta \quad (2\text{-}2)$$

Similarly, the error in the *y* coordinate which orthogonal to the print direction is mainly determined by the angular deviation of the drop and can be represented by the equation 2-3:

$$\Delta y \approx s\sec^2\theta\cdot\Delta\theta \quad (2\text{-}3)$$

In general, the translation velocity is 0.1 m/ s, the drop frequency is 10 to 20 kHz, the drop velocity is 6 to 8 m/ s, the distance between the print heads to the substrate is 1 to 5 mm, and the angular drop placement deviation is 0.005 rad. Using these parameters, the expected error in the ejected drop placement is 5-10 μm which correlates well to measure printed droplets from a multi-ejector print head.

2.1.3 Ejection Process

The ink-jet printing process consists of five steps as shown in Fig. 2-4: (1) ejection from the inkjet nozzle, (2) flight, (3) impact, (4) spreading, and (5) drying.

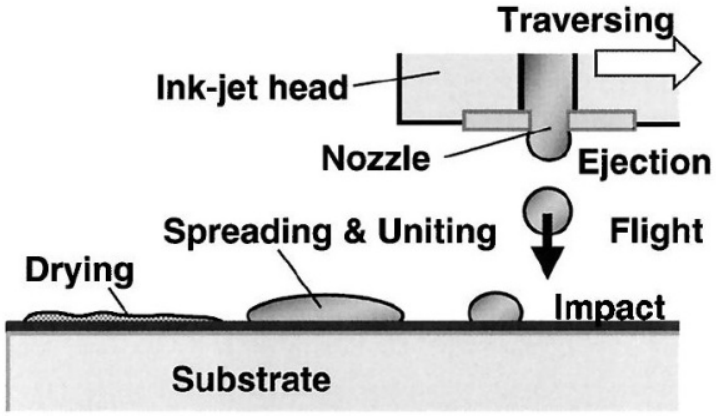

Fig. 2-4 Processes of film formation in inkjet deposition.

2.1.4 Droplet Landing

A droplet strikes a solid surface and exhibits complicated behaviors as shown in Fig. 2-5. A droplet spreading onto the substrate consists of an initial spontaneous spreading for a short time and then a wet spreading for a longer time. A droplet that hits a solid surface expands in the radial direction and reaches a maximum diameter D_{cmax}. If the surface energy is excess at this time, the droplet diameter decreases as liquid flows toward the center of the droplet. This is called recoiling. Then the droplet might rebound when the energy is excess. If there is still much energy, the droplet vibrates, repeatedly increasing and decreasing it diameter. Time between these expansions and contractions is several microseconds, and the droplet settles into a nearly stable shape when the energy is dissipated.

The droplet shape then slowly changes to the final profile with the minimum surface energy. This is called as “wet spreading.” The contact angle if the droplet becomes a static one and the droplet diameter asymptotically approaches the final equilibrium diameter (D_f) the time between the beginning of wet spreading and the attainment of the D_f ranges from several seconds to tens of seconds.

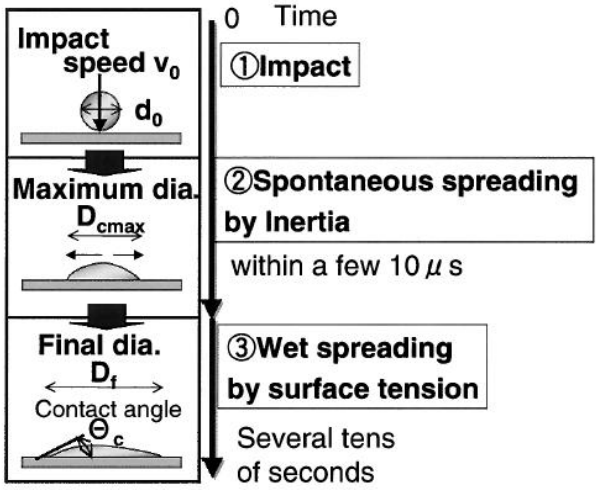

Fig. 2-5 Behavior of a developing droplet during impact on a substrate.

2.1.5 Spontaneous Inertial Spreading of Droplets

The spontaneous spreading of a liquid droplet has been investigated in various field of engineering. A model is a semi-empirical formula intended for the droplets with the size of those produced by an ink-jet printer.[7] The relation between the maximum diameter (D_{cmax}) and viscosity (μ) was examined by using the equation:

$$\frac{D_{c\max}}{d_0} = 1 + 0.48We^{0.5}\exp[-1.48We^{0.22}\,\mathrm{Re}^{-0.21}] \qquad (2\text{-}4)$$

Where We and Re are Weber number and Reynolds number, respectively.

2.1.6 Coffee Ring Effect

In the theory, an outward flow in a drying droplet of liquid is produced when the contact line is pinned so that liquid is removed by evaporation as shown in Fig. 2-6. This flow is capable of transferring 100% of the solute to the contact line and thus accounts for the high perimeter concentration of many strains. The evaporation flux has a universal form that depends only on the shape of the droplet. In the evaporation process, liquid molecules interchange rapidly between the surface, the air, and the vapor. As the distant air is not

saturated, the vapor diffuses outward from the surface to the droplet.

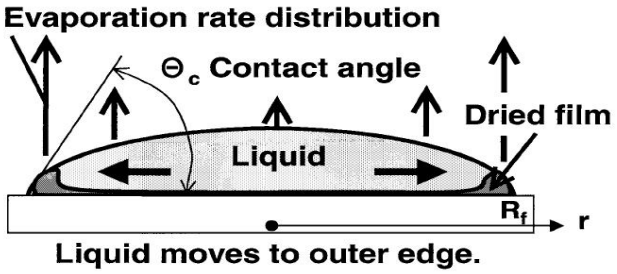

Fig. 2-6 Deegan's model for coffee ring effect.

The vapor quickly approaches the steady-state diffusion equation:

$$\nabla^2 \Phi(r) = 0 \qquad (2\text{-}5)$$

where Φ(r) is a steady-state concentration profile. The derivative at the surface gives the evaporating flux,

$$J(r) = -D\nabla\Phi(r) \qquad (2\text{-}6)$$

where D is the diffusion coefficient of the vapor in air. For the droplet with the contact angle θ_c on the substrate, the evaporation flux can be expressed by Eq.2-7,

$$J(r) \propto (R_f - r)^{-\lambda} \qquad (2\text{-}7)$$

Where $\lambda = (\pi - 2\theta_c)/(2\pi - 2\theta_c)$ and $R_f = D_f/2$. The contact angle decreases and towards zero, while λ approaches to 1/2. We noticed by this theory that the evaporating flux J becomes uniform when the contact angle is $\pi/2$. The evaporation-flux distribution in the radial direction is shown in Fig. 2-7 for various contact angles with respect to the substrate.

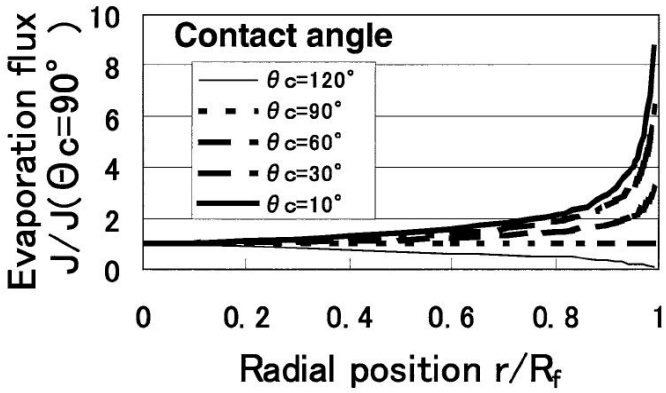

Fig. 2-7 Evaporation-flux distribution for various contact angles.[8]

When the contact angle of droplets at the edge is less than 90°, where could get the higher evaporation rate. A large amount of solutes might accumulate at the edge as flow from the central area replaces the evaporating liquid.

2.1.7 The Marangoni Effect

The Marangoni flow is generated form a surface tension gradient.[9] During evaporation, evaporative cooling reduces the temperature of droplet-surface non-uniformly. The temperature at the liquid-air interface on the top center of the droplet is the lowest due to a longer thermal conduction path, and the surface tension is the highest there. This phenomenon produces an inward flow near the droplet surface, whose shear stress balances the Marangoni stress, i.e., the surface tension gradient.

When using a mixture of a low- and a high-boiling solvent, the composition at the contact line will shift toward a higher fraction of higher-boiling solvent than in the buck, due to the increased rate of evaporation at the edge.[10] As the rate of evaporation at the contact line decreases, a surface tension gradient is established.

2.1.8 Pattern Design

A schematic diagram of the design of pixels and printed dots are shown in Fig. 2-8. The objects are defined as the number of pixels in the x and y directions, which are referred to as the process (printing) direction and normal direction, respectively, in this study. In designing the object, it is possible to generate two images with the same dimensions but different design resolutions. In printing, one printed droplet from the print head corresponds to one pixel.

The printed results with different design resolutions are not the same due to the overlap of dots. The overlap of the dots is determined from the diameter of the droplet, the spreading of the droplet on the substrate, and the printing resolution. The printing resolution is typically expressed as dots per inch (DPI). The center-to-center distance between two dots, hereafter called the dot pitch (DP), is solely dependent on the DPI. If the dot diameter is known, the dimensions of printed results can be calculated by the following equation,

$$W = (n-1)\times DP + D \qquad (2\text{-}8)$$

Where W is the width, n is the number of pixels, DP is the dot pitch defined by 25400 um/DPI, and D is the diameter of the printed dot.

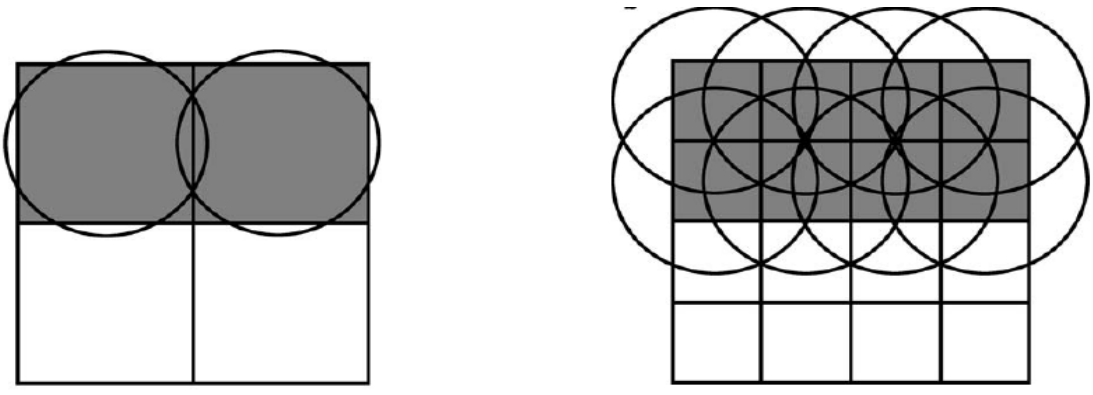

(a) (b)

Fig. 2-8 Schematic diagram of the designed pixels printed dots: (a) a design with a resolution of 2 x 2 pixels and (b) a design with a resolution of 4 x 4 pixels.

For example, if the dot diameter is 100 μm with printing resolution 500 DPI, there exists 196 dots.

2.2 Radiometry and Photometry

2.2.1 Radiometry

Radiometry is a science which is used to measure the radiation and principally deals with the radiant energy of any wavelength. No matter what kinds of optical system design, the purposes are receiving and transmitting the radiation or communication energy. Therefore, the radiation should be quantified and defined clearly. The fundamental radiometric quantities are shown in Table 2-1.

Table 2-1 Radiometry quantities

Quantity	symbol	Definition	Typical Units
Radiant Energy	Q		*Joule* (*J*)
Radiant Flux	φ	dQ/dt	*Watt* (*w*)
Radiant Intensity	*I*	dφ / dw	*Watt*/sr
Radiance	*L*	dφ / cosθ dA dw	*Watt*/sr · m^2
Irradiance	*E*	dφ / dA	*Watt*/ m^2
Radiant Exitance	*M*	dφ / dA	*Watt*/ m^2

The *Q* denotes the propagating energy of electromagnetic radiation, and its basic unit is the Joule. Sometimes, the amount of photons is also defined as the radiation energy, and the energy of a single photon is $h\nu$.

The radiant flux is the rate of flow of the energy with respect to time, *dQ/dt*, and the unit is Watt (*W*). The recommended symbol for power is *φ*. The radiant intensity is power per unit solid angle**,** and the unit is *W/sr*. One steradian (sr) is the solid angle that, having its vertex in the center of sphere, cuts of an area on the surface of the sphere equal to that of a square of side of length equal to the radius of sphere. The intensity is the derivative of the power with

respect to the solid angle, *dφ/dw*. The symbol is *I*.

The radiance is power per unit projected area per unit solid angle, and the unit is W/m^2sr. Radiance is the flow of the power with respect to the solid angle and projected area, dφ/dωdAcosθ, where θ is the angle between the surface normal and the specified direction.

The Irradiance is measured in W/m^2. Irradiance is the power per unit area incident from all direction in a hemisphere whose base is that surface. The symbol is *E*, and it is the derivate of the power with respect to area, *dφ/dA*. A similar quantity is radiant exitance, which is the power per unit area leaving a surface to a hemisphere whose base is that surface. The symbol is *M*.

2.2.2 Photometry

Photometry is the measurement of light which is defined as electromagnetic radiation that is detectable by the human eye. This range corresponding to wavelength is 380 to 830 nanometer (*nm*). Unit symbols are subscripted with *v* to denote visible, and unit names are prefixed with the term luminous. The unit of luminous flux (φ_v) is called a lumen (*lm*). The fundamental photometric quantities are similar to the radiometric as shown in Table 2-2.

Table 2-2 Photometry quantities

Quantity	symbol	Definition	Typical Units
Luminous Energy	Q_v		$lm \cdot s$
Luminous Flux	φ_v	dQ_v/dt	*lumen (lm)*
Luminous Intensity	I_v	$d\varphi_v / dw$	lm/sr
Luminous	L_v	$d\varphi_v / \cos\theta\, dA\, dw$	$lm/sr \cdot m^2$
Illuminance	E_v	$d\varphi_v / dA$	lm/m^2
Luminous Exitance	M_v	$d\varphi_v / dA$	lm/m^2

The only difference between radiometry and photometry is that the radiometry includes the entire optical radiation spectrum, while photometry is limited to visible spectrum as defined by response of human eye. Fig. 2-9 shows the both measurement system.

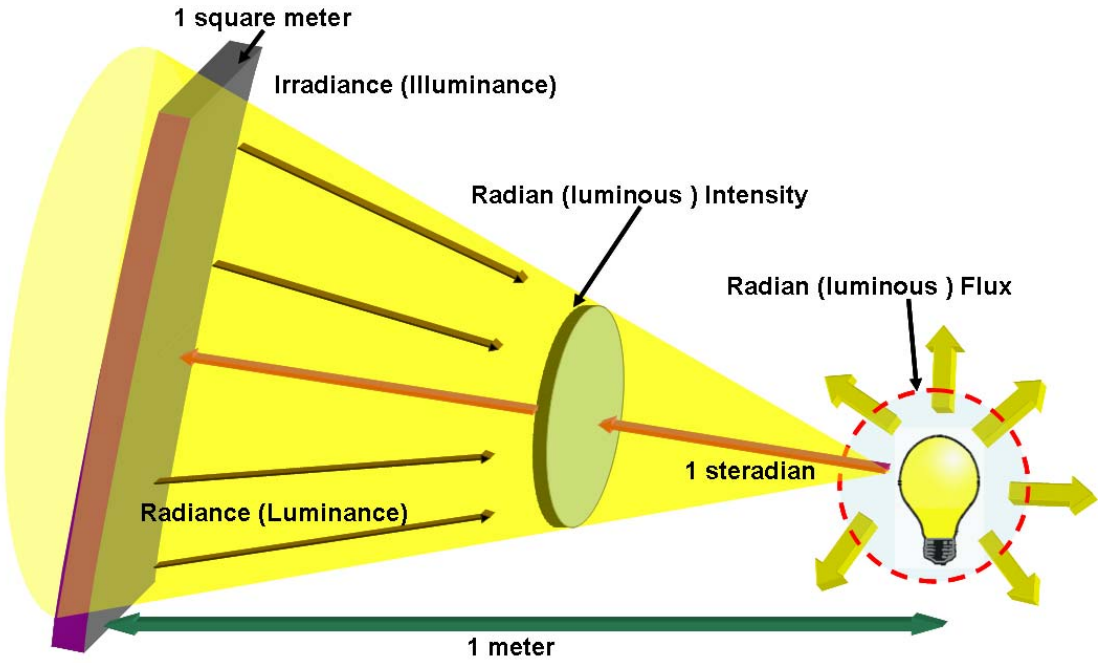

Fig. 2-9 The unit of radiometric and photometric.

From the lumen definition, there are 683 lumens per watt at 555 nm. This is the wavelength that corresponds to the maximum spectral responsivity of human eye. The conversion from watts to lumens in any other wavelength involves the product of power (*watts*) and the $V(\lambda)$ in the wavelength of interest. The luminous flux in any wavelength can be calculated by the following equation:

$$\varphi_v = 680 \int V_\lambda(\lambda)\varphi_\lambda(\lambda)d\lambda \qquad (2\text{-}9)$$

Where φ_v is the luminous flux, $\varphi_\lambda(\lambda)$ is the corresponding radiant spectrum of radiation source, and $V_\lambda(\lambda)$ is the photopic spectral luminous efficiency function as shown in Fig. 2-2.

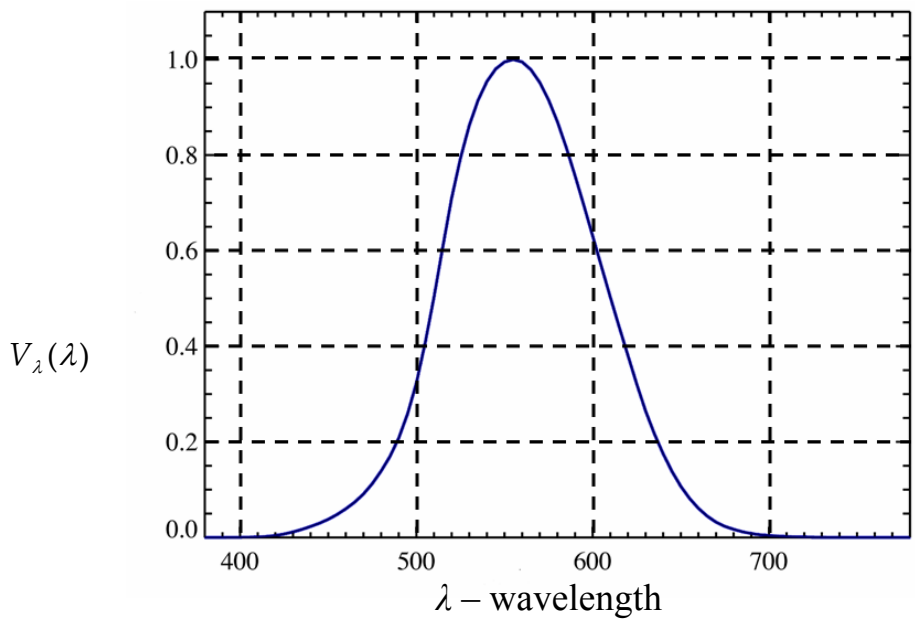

Fig. 2-10 Normalized human visual response function in photopic state.

In both measurement systems, the term *Watt* refers to the energy per unit time generated by radiation source. Thus, it is possible to define two different measurements with the same units. The term radiant efficiency, with units *W/W*, refers to the energy conversion efficiency of radiation source in converting electrical power into radiant flux. The term luminous efficiency, with unit *lm/W*, refers to the energy conversion efficiency of the light source in converting electrical power into luminous flux. The term luminous efficiency, with unit *lm/W*, refers to the ratio of luminous flux to radiant flux generated by the light source.

Chapter 3

Experiment and Optical Design

Ink-jet printing technology can be used to simplify the fabrication in light guide plate. To develop a reliable printing process, the ink-jet system can be divided into three critical components: the head, the substrate and the inks. Strong correlation between these three factors mainly determines the quality of microlens and substantial performance. In this chapter, the fabrication and the flow of optical design will also be described.

3.1 Process Design and Schemes

In this research, we developed a novel high-precision multi-head, multi-nozzle inkjet printer that utilizes graphical printing to implement a 7-inch 16:9 format light guide plate for LCD application. Therefore, this topic is divided into two main parts: fabrication process and optical design. In the fabricaion process, we will discuss the three critical components: the printed head, the substrate and the inks to create the microlens. The microlens was used to deflect the ray direction with 3 main controllable factors: shape, sizes, and arrangement. In optical design, we use various values of fill factor to control the light distribution. The combination of the fabrication and the optical design is illustrated in Fig. 3-1.

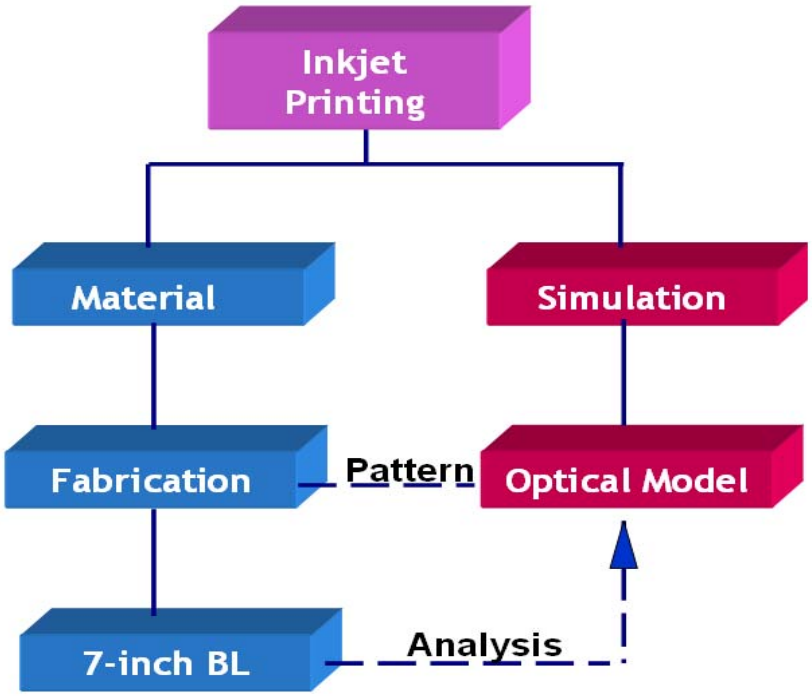

Fig. 3-1 Flow chart of the ink-jet printing process

3.2 Fabrication Process

3.2.1 Material and Substrate

The relationship between material and substrate might affect the form of the microlens seriously. The material we used is UV-curing optical epoxy resin. The refractive index is 1.510. The glass transfer temperature of the material is about 156 ℃, and the solid content is 96% with 93% transmittance. The PMMA substrate which is chosen is coated with Perfluorinated, resulting in hydrophobic surfaces. The contact angle between the droplet and the substrate affects the shape of microlens, and it is controlled by the surface tension between the lens material, the material of the substrate, and the environment. Fig. 3-2 shows the contact angle equilibrium, where the contact angle (α) in equilibrium for an ink drop on various surface treatments is related to the interfacial tension equation, called Young's equation,[11,12]

$$\gamma_{S/A} = \gamma_{S/L} + \gamma_{L/A}\cos\alpha. \quad , \qquad (3\text{-}1)$$

Where $\gamma_{S/A}$, $\gamma_{S/L}$, and $\gamma_{L/A}$ are the interfacial tension of the interfaces between the air, the liquid, and the substrate.[13] Fig. 3-3 (a)-(d) show the lens profiles where the resins are dropped on the PMMA with non-treatment surface, the hydrophobic surface, the low-power etched surface (Reactive Ion Etching), and the high-power etched surface, respectively. Through changing surface characteristics, such as ion-etch and perfluorine coating, the contact angle can be controlled. To evaluate those parameters related to the surface free energy, Eq. 3-2 is derived from Young's equation

$$\gamma_{L/A}(1+\cos\alpha) = 2(\gamma_{L/A}\gamma_{S/A})^{\frac{1}{2}} e^{-\beta(\gamma_{L/A}-\gamma_{S/A})^2}, \qquad (3\text{-}2)$$

Where β is an empirical constant with an average value of 1.06 x 10^{-4} (m^2mJ^{-1}).[14] Here the surface tension $\gamma_{S/A,}$ of the PMMA with perflurine hard coating we used is substantially adopted as 31 dyne/cm. Thus, the relation between the surface tension of ink material and the contact angle is shown in Fig. 3-4, where the experimental measurement has close agreement with the analytic curve.

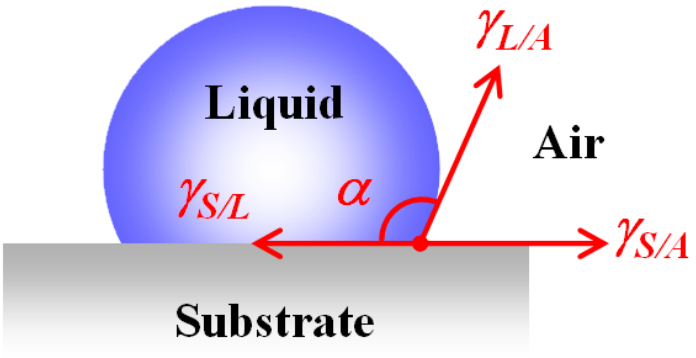

Fig. 3-2 The contact angle and the tensions of the interfaces.

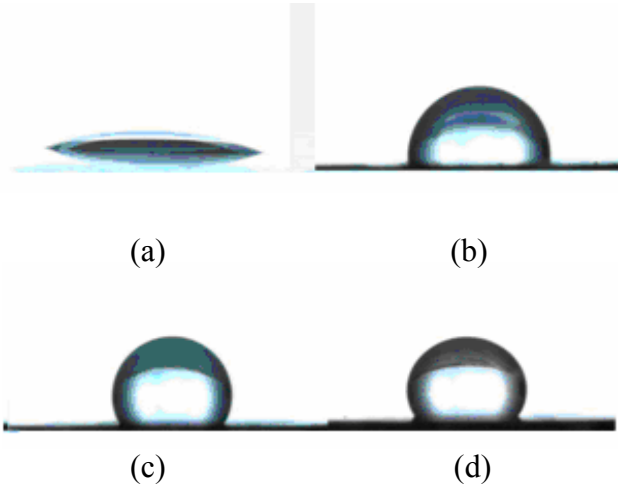

Fig. 3-3 The shape of microlens on the PMMA with: (a) nontreatment surface, (b) perfluorine coating surfaces, (c) low-power RIE, and (d) high-power RIE

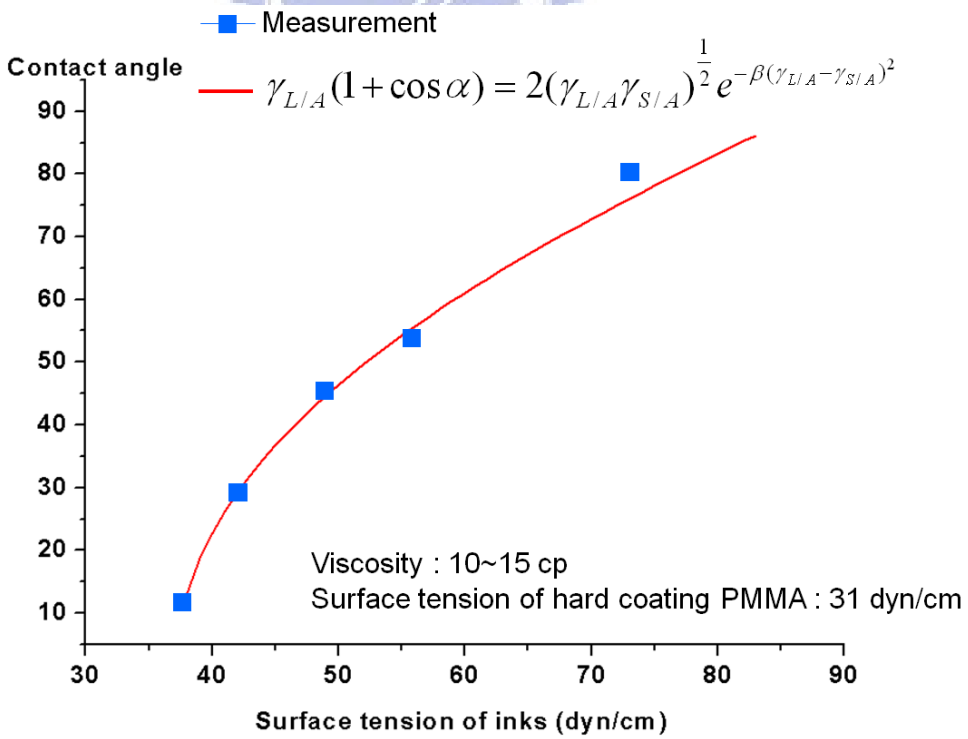

Fig. 3-4 The relationship between contact angle and the surface tension of ink

3.2.2 Ink-jet printing System

Ink-jet printer, Litrex 70, consists of a piezoelectric-based print head, an automated XY-table (20cm*20cm), and a controlling computer for the programmed fabrication process. The piezoelectric printing head for our system (SE-128) has 128 number of nozzles with 38 um nozzle diameter which is compatible with organic solvents, UV curable resins, and Electronic fluids. The fluid viscosity for the printing head should be controlled in the range of 8~13-cp. The printing system Litrex 70L and the photograph of the print-head are shown in Fig. 3-5.

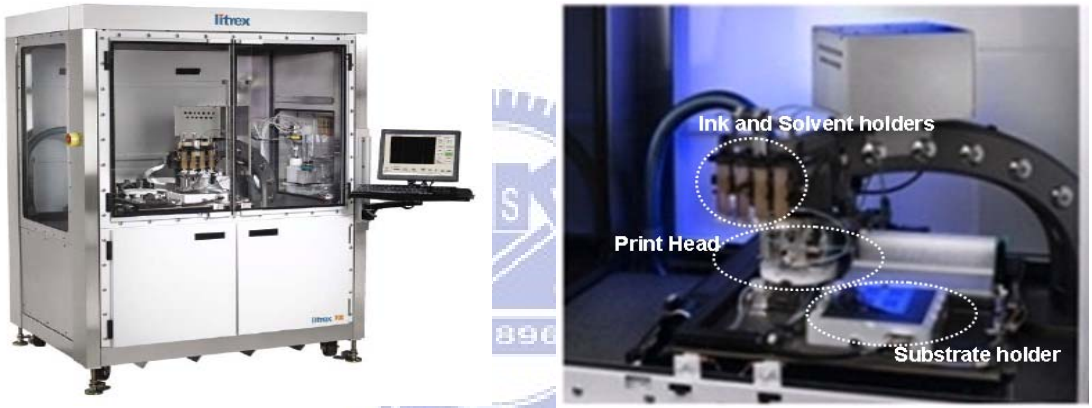

(a) (b)

Fig. 3-5 (a) The printing instrument Litrex 70L and (b) the key components of the printing system.

To enhance the performance of print-head, isopropyl alcohol (IPA) or propylene glycol monomethyl ether acetate (PGMEA) was used to develop the droplet calibration and droplet analysis. The droplet checking process was monitored with a built-in program. Besides, driving voltage and pulse time of nozzle are another parameters affecting the formed, position, and arrangement of diffusing dots. Weaker driving voltage results in bad jetting and collimating. Although stronger driving voltage makes better collimating, the form might destroy. Similar to driving voltage, the pulse time have to finding the matching value to make the form and position stable, previous mention as shown in Fig. 3-6. After setting up, the

printing process was ready for proceeding.

During IJP fabrication that can control microlens size and pitch, desirable drop patterns and sizes are formed with very high speed. A fabrication process on the 20 cm*20 cm substrate is no more than 10 seconds.[15] Fig. 3-7 shows the comparison of radius of the droplets with different pulse time, (a) 20 um (b) 25 um (c) 33 um (d) 40 um, besides, the variability of the microlens size is subjected the aggregation of the droplets, as shown in Fig. 3-8 . The radius of the maximum diffusing dots is 60 um, the height is 38 um; and the minimal radius is 20 um, and height is 13 um in this experiment. Finally, the arrangement of the microlens array can be fabricated precisely with radius of 30 um, and Fig. 3-9 shows different arrangements of diffusing dots. Fig. 3-9 (a) and (b) show the pitch of rectangular array with 150 um and 70 um. Fig. 3-9(c) shows the pitch of hexagonal array with 80 um. Obviously, it is convenient and precise to fabricate the microlens array.

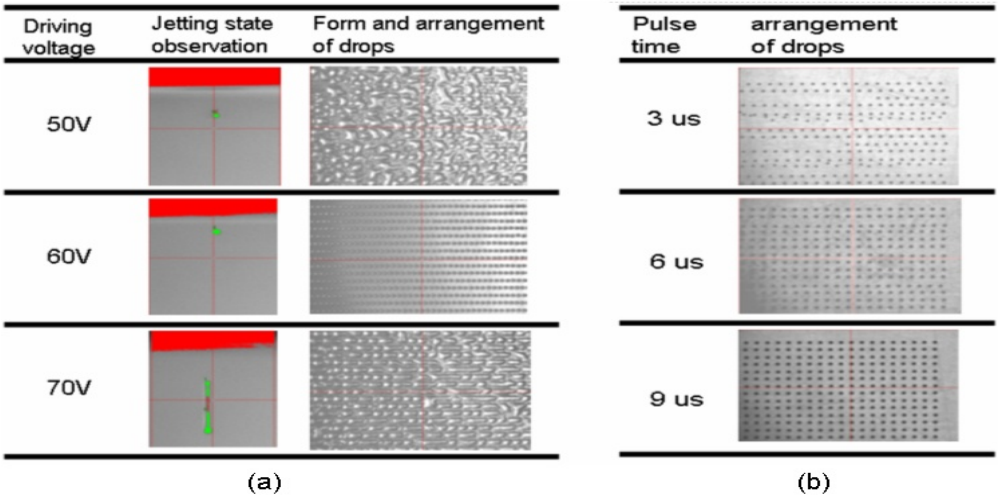

Fig. 3-6 Optical-microscope pictures of an array of drops with (a) driving voltage and (b) pulse time

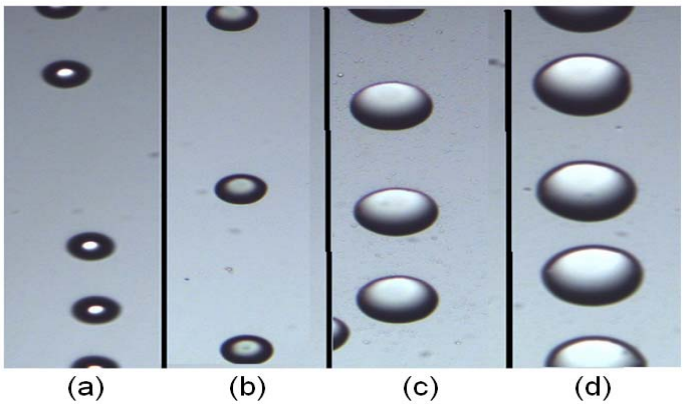

Fig. 3-7 The comparison of the drop radius (a) 20 um-3 us (b) 25 um-5 us (c) 33 um-7 us (d) 40 um-9 us

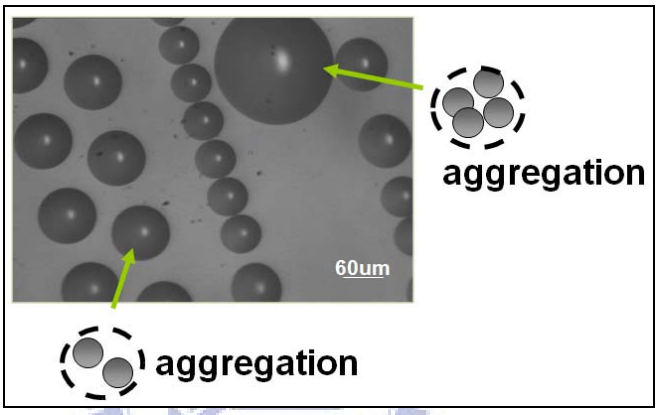

Fig. 3-8 The comparison of the microlens size

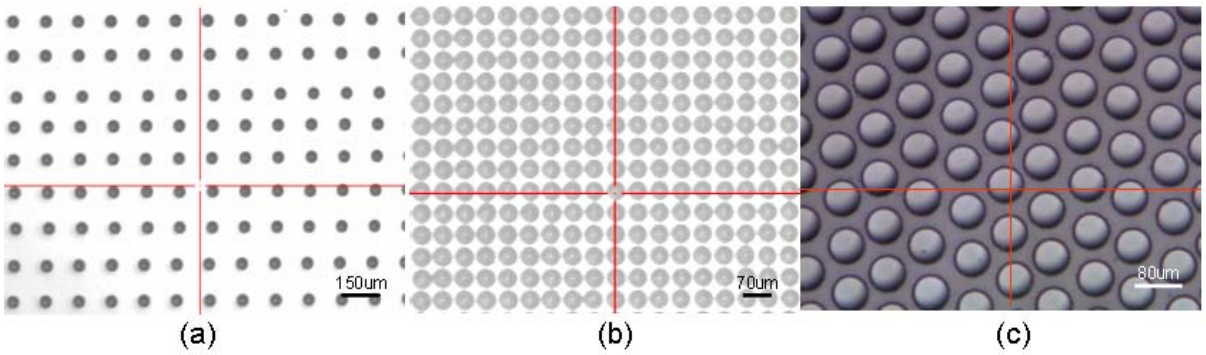

Fig. 3-9 OM pictures of an arrangement of diffusing dots, here are different pitches and arrangement (a) 150 um (b) 70 um (c) 80 um

3.3 Optical Design

3.3.1 Design Concept

In this research, the microlens array under the LGP plays the role as the lenslet microdeflector. In a dummy LGP, because of the total internal reflection (TIR), most of the incident light from the source is guided inside the PMMA plate, and there is almost no flux propagating out from the output surface. The lenslet microdeflector under the PMMA plate redirects some of the TIR rays and extracts the light outside the LGP. However, the unit profile, distribution, and refraction index of microlens array affect the efficiency of extracted light. The purpose of our LGP is to use the Ink-jet lenslet microdeflector to couple out the guided rays and uniformize the light distribution of the output surface. In order to describe the optical performance, we define the extraction efficiency: [16]

$$\eta_e = \frac{\Phi_{ext}}{\Phi_{in}}. \quad (3\text{-}3)$$

Fig. 3-10 describes the corresponding symbols, where Φ_{ext} and Φ_{out} indicate the incident flux and extracted flux of the unit region (blue region). Φ_{TIR} means the flux which is not extracable, and guided with TIR into next unit region. We descritize a 7-inch LGP into 10×10 unit regions, and optimize each bottom structures to achieve the Φ_{ext} that is the same from every unit region.

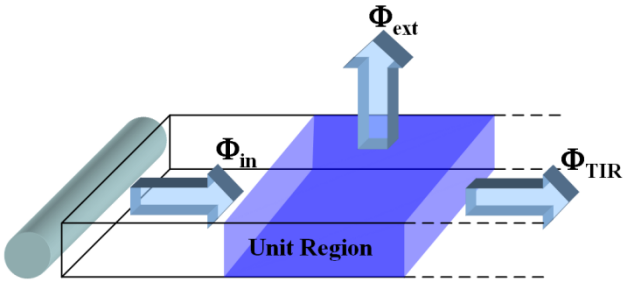

Fig. 3-10 Schema of light flux in the LGP

In our design, the microlens with 50 um diameter, 5 um sag, 65 um radius of curvature, and refractive index n=1.510 is chosen for the leslet microdeflactor, and the arrangement density of the microlens array is the variant factor for optimization. Fill factor is applied to describe the arrangement density, and defined as

$$\rho = \frac{A_{lens}}{A_{unit}}, \qquad (3\text{-}4)$$

where A_{lens} and A_{unit} are the area of lens and unit, respectively. Fig. 3-11 shows their corresponding meanings. Theoretically, the higher fill factor causes more rays coupled out the LGP. According to Monte Carlo ray tracing, extraction efficacy versus fill factor in our system is shown in Fig. 3-12. From this figure, we see the trend of the function is almost linear. This curve provides a useful function that correspond the lens arrangement to the optical properties. Thus, we can arrange the microlens in different fill factors from the regions near the light source to the final region.

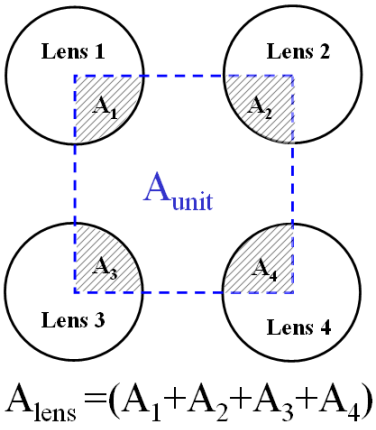

Fig. 3-11 Definitions of the two areas in fill factor

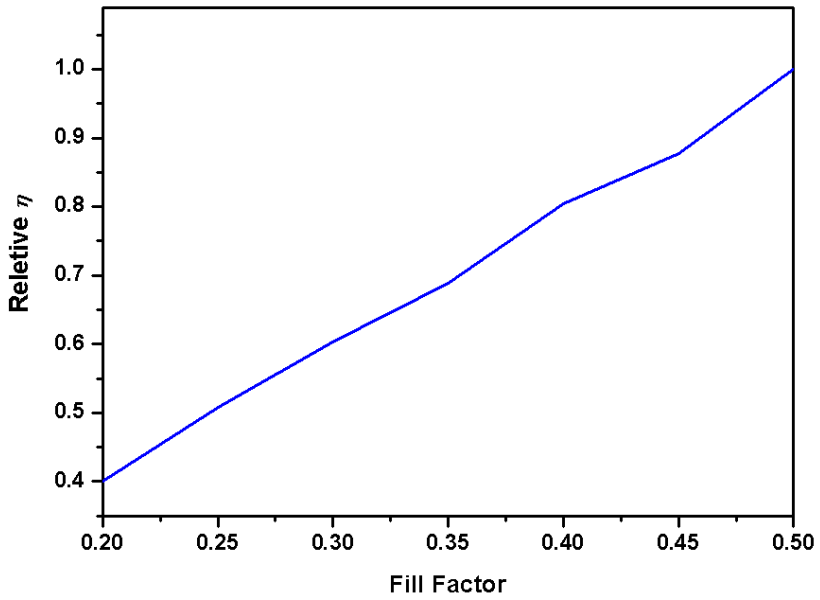

Fig. 3-12 Extraction efficiency versus fill factor

3.3.2 Optical Simulation

As we know, we want to design the pattern with different distributions of fill factor. By using Monte Carlo ray tracing, the extraction efficiency is directly proportional to the fill factor. This relationship provides a useful data base connecting the lens arrangement to the optical properties. Therefore, the flow of design is shown in Fig. 3-13. The designed optimize the output uniformity of this system, the false position method is applied to find out the solution. The designed distribution of fill factor is shown in Fig. 3-14.

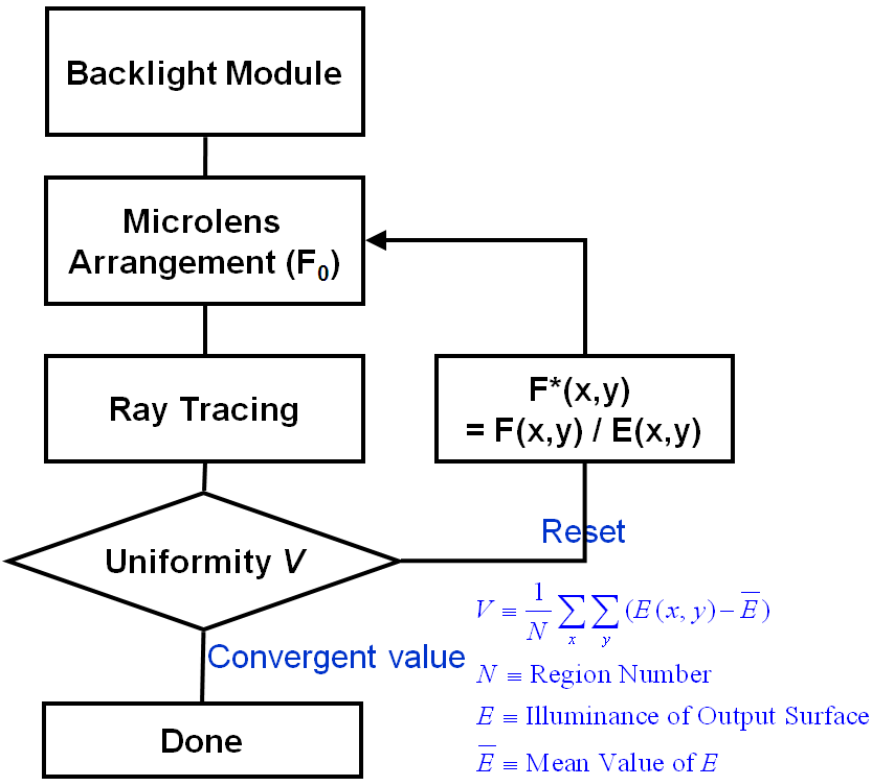

Fig. 3-13 Flow of the optimization.

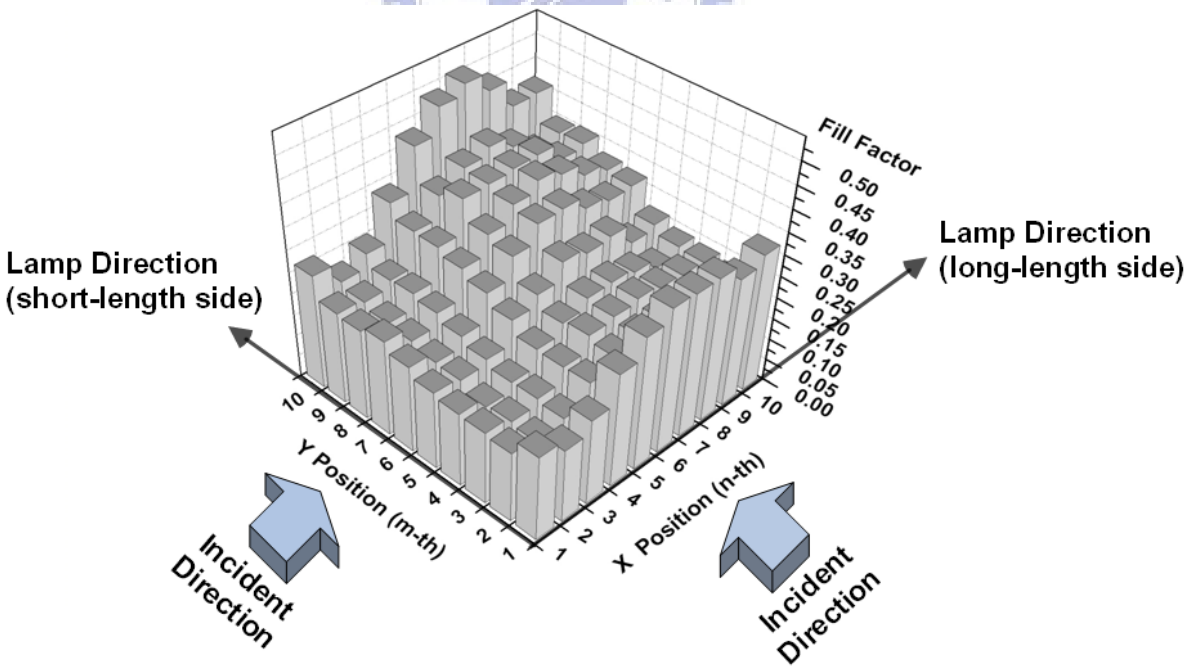

Fig. 3-14 The optimized fill factor distribution

Chapter 4

Result and Discussions

4.1 Experimental Result

4.1.1 Analysis of Microlens Array

The fabricated LGP with the designed pattern is shown in Fig. 4-1.Therefore, the experimental results verified ink-jet technology applicable to LCD backlight system. Fig. 4-2 shows the 3-D pattern by interference meter, the diameter of microlens is 50 um, and the height is 4 um, and the aspect ratio is 0.08. Moreover, ink-jet process is able to reproduce accurately and quickly within the same shape.

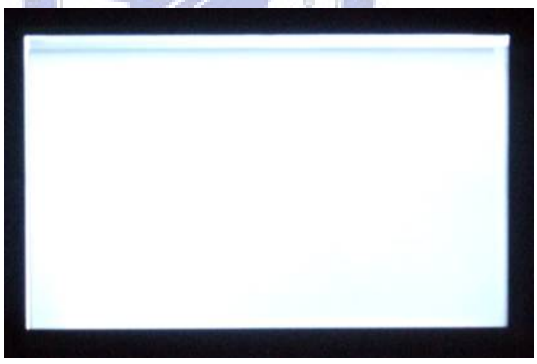

Fig. 4-1 The 7-inch LGP with ink-jet microlens array

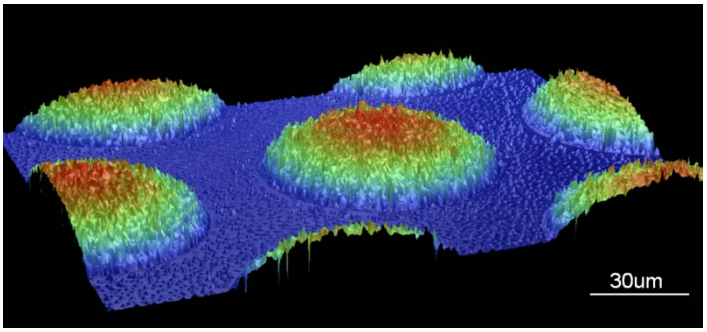

Fig. 4-2 The microlens array by interferometer

To evaluate the accuracy of the printed microlens array, we take five points on the diagonal of the 10×10 elements to measure the lens periods, as shown in Fig. 4-3. The comparisons between the ideal and experimental results, where lens array had the fill factor from 0.2-0.5 and the errors of lens pitch are under 6 %, as shown in Fig. 4-4 and list in Table 4-1. The arrangements of microlens array are well defined by computer graphic layout.

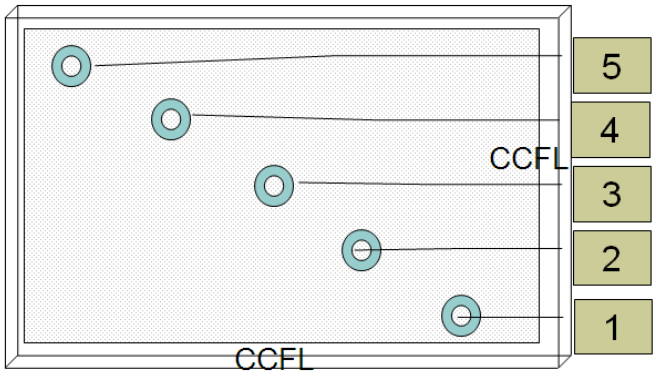

Fig. 4-3 Measurement points

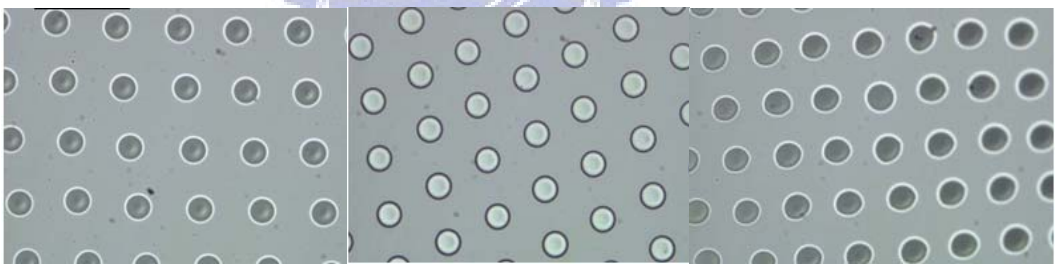

(1) (2) (3)

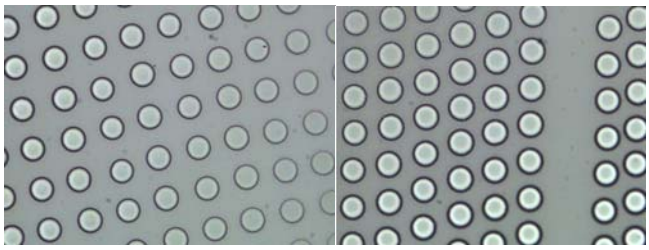

(4) (5)

Fig. 4-4 The microlens array of each reference point

Table 4-1 Evaluation of ink-jet accuracy

Position	5	4	3	2	1
Ideal Period (um)	120	105	97	85	75
Measurement (um)	125	113	99	87	80
Error (%)	6	6	2	3	6

To complete ink-jet process of 7 inch LGP would need 650000 droplets, so the variability of microlens, which might affect the optical performance, has to be discussed. To evaluate the variability of diameter of mircolens, we use optical microscopy to measure the diameter of microlens on the LGP. The result was concluded and shown in Fig. 4-5, where 500 microlens were arbitrarily sampled, and the ideal diameter is 50 um. The variability is under 5% for 90% microlens. Obviously, the designed microlens was accurately coated by the ink-jet technology.

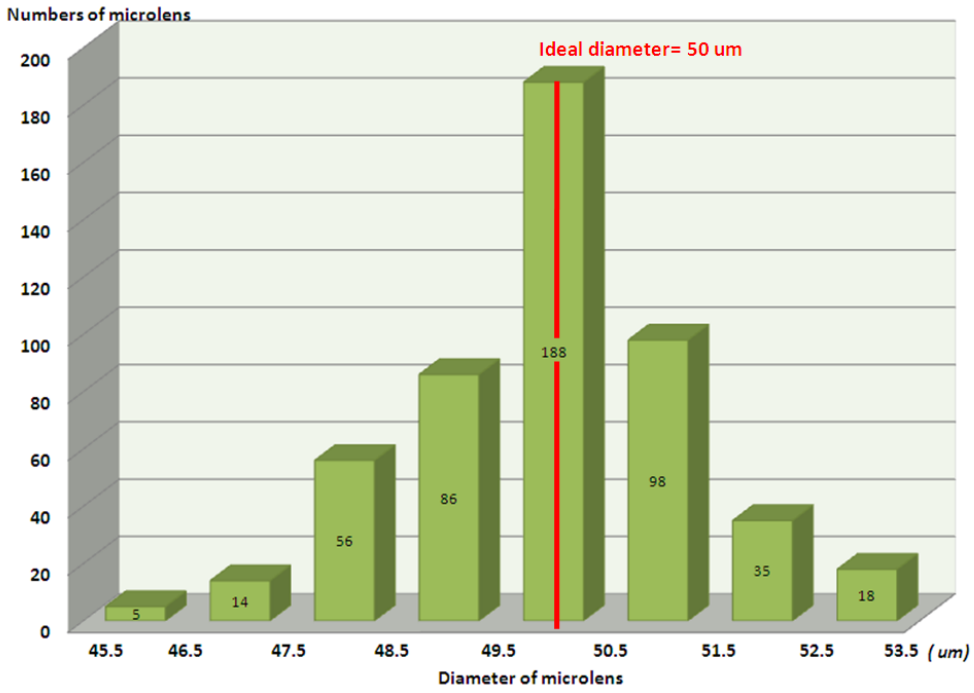

Fig. 4-5 Evaluation of variability of diameter

4.2 Optical Measurement

4.2.1 Brightness and Uniformity

As we know, the uniformity and the brightness are the key parameters of judgment of LGP. To compare brightness and uniformity of an ink-jet printed LGP with conventional LGP, we used the same backlight structure, L type CCFL, diffusing white plate, diffusing sheet, and BEF.

The optical properties of the LGP are measured and analyzed. The luminance distribution is measured by luminance camera, and the result is shown in Fig. 4-6 . The 9-point uniformity, defined as

$$Uniformity = \frac{L_{\min}}{L_{\max}} \times 100\%, \quad (4\text{-}1)$$

is over 82% which is higher than the conventional backlight (<80%). In the definition, $L_{\min}$ and $L_{\max}$ are the minimum and maximum luminance of the 9 measured points. Therefore, measurements of cross section of center line indicate the average luminance of the whole LGP which are 2477 nits by Ink jet printed and 2569 nits by conventional LGP, as shown in Fig. 4-7. Finally, we can say the optical performances are comparable with the conventional backlight.

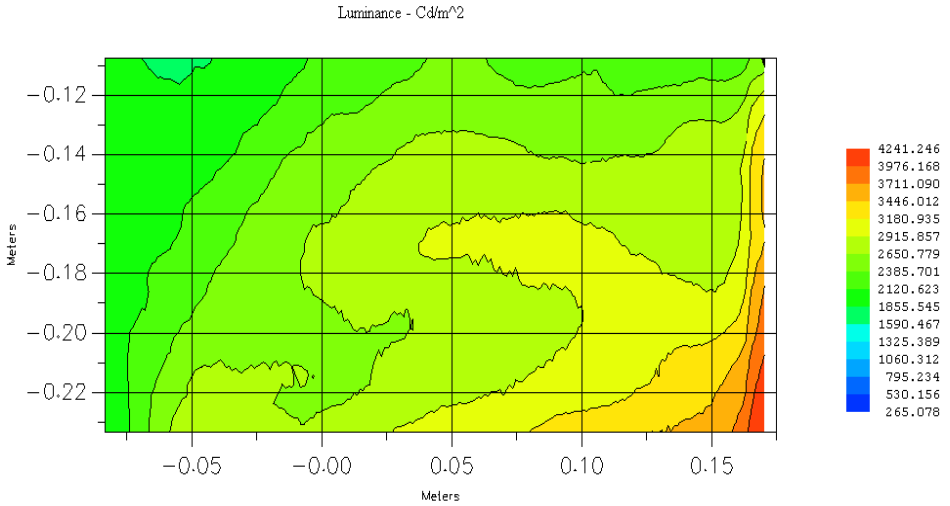

(a) Conventional LGP

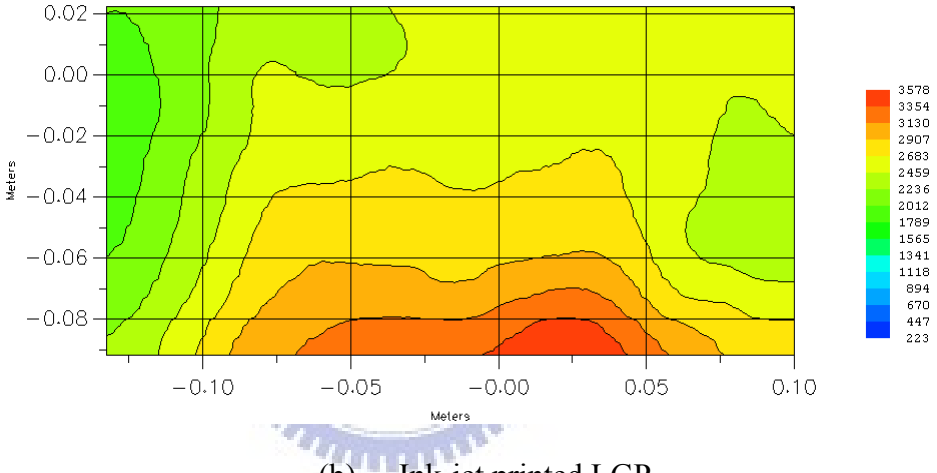

(b) Ink-jet printed LGP

Fig. 4-6 Light distribution of front view

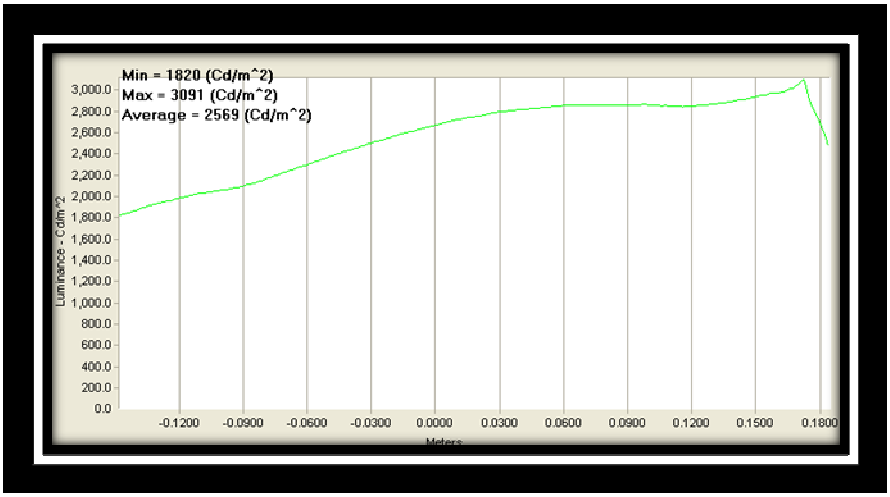

(a) Conventional LGP

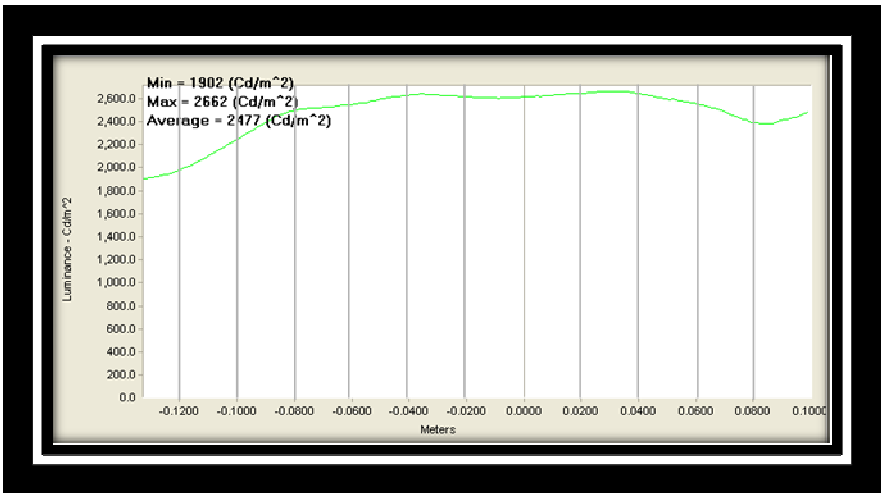

(b) Ink-jet printed LGP

Fig. 4-7 Light distribution of center light

4.2.2 Yellowish Effect

Visually, yellowish is associated with scorching, soiling, and general product degradation by light, chemical exposure, and processing. The yellowish effect would affect the brightness seriously. .Because the material we used is UV curable epoxy, the epoxy must be exposed by 365 UV light. The fabricated process might cause the PMMA substrate yellowish. Fig. 4-8 displays the image of backlight with a LGP by using ink-jet printed and a conventional LGP, besides, we pick 9 reference points to be detected by luminance camera. The result of measurement is shown in Table 4-2. The color coordinate of ink-jet printed is close to yellow region, and the color coordinate of conventional LGP is close to blue region, as shown in Fig. 4-9.

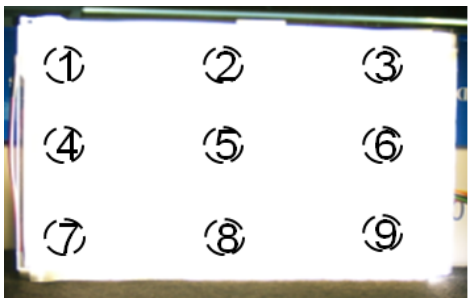

(a) Conventional LGP

(b) Ink-jet printed LGP

Fig. 4-8 The image of LGP

Table 4-2 The x-y color coordinate of reference points

Conventional LGP	x	y	Ink- jet printed	x	y
1	0.269	0.274	1	0.293	0.292
2	0.267	0.275	2	0.296	0.296
3	0.268	0.277	3	0.298	0.299
4	0.268	0.275	4	0.294	0.293
5	0.266	0.279	5	0.297	0.297
6	0.268	0.277	6	0.299	0.3
7	0.269	0.278	7	0.296	0.294
8	0.267	0.278	8	0.299	0.299
9	0.269	0.282	9	0.302	0.304
Ave.	0.267	0.277	Ave.	0.297	0.298

According to American Society for Testing and Material (ASTM), yellowness index is calculated as following:

$$YIE313 = \frac{100(C_X X - C_Z Z)}{Y} \quad (4\text{-}2)$$

Where X, Y, and Z are CIE Tristimulus values and the coefficients depend on illuminant and observer as indicated in Table 4-3. Yellowness index might be calculated illuminant D65 and C.

Table 4-3 The dependence of coefficients on illuminant and observer

Coefficients	C/2°	D65/2°	C/10°	D65/10°
Cx	1.2769	1.2985	1.2871	1.3013
Cz	1.0592	1.1335	1.0781	1.1498

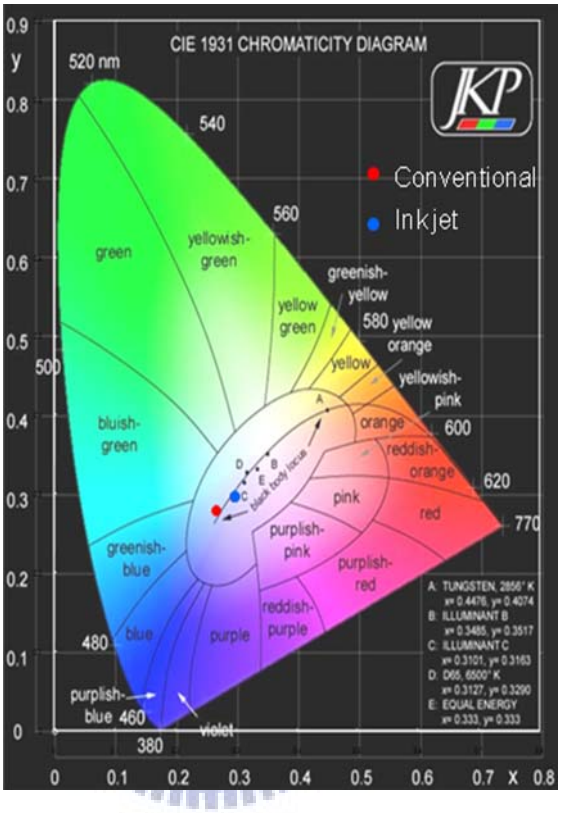

Fig. 4-9 CIE 1931chromaticity diagram

The Tristimulus values of conventional LGP are x=0.267, y=0.277, and Y=100, and the values of ink-jet LGP are x=0.297, y=0.298, and Y=100.Using these values, the ASTM formula yields YI=-51.6 for conventional LGP and YI=-16.9 for ink-jet printed LGP. Positive yellowness values indicate presence and magnitude of yellowness, while a negative yellowness value indicates that a material appears bluish.

Chapter 5

Conclusions and Future Work

5.1 Conclusions

The ink-jet printed microlens array for backlight applications was demonstrated in a 7-inch LGP. The method exhibited several superiorities over traditional methods. A 20×20 cm^2 LGP can be dropped within 10 seconds, so it has potential to apply on high-throughput mass production. The optical patterns can be precisely coated on the substrate. Furthermore, all the process is kept with room temperature. It is not feasible to accomplish the complex diffusing structure which is constrained by the conventional molding approaches. Compared with the traditional products, the demonstrated 7-inch CCFL LGP shows required brightness and uniformity. The result of this study shows the Ink-jet technology has potential to apply on LCD backlight products.

5.2 Future Work

Future research is obviously required, but this is an exciting first step. Among the many topics to be explored in future, some important ones can be listed as follows.

1. An important part for future research will be how to reduce the yellowish effects. Because the material we used is UV curable epoxy, which must be cured by UV light, the yellowish effects of the PMMA substrate will be caused in the exploring process. The improved material or fabricating process should be considered and pursued.
2. An additional interesting avenue of investigation is to use a new type optical mechanism, for example, the nanoparticle-mixed the material.

The potential of inkjet technology in the display clearly needs further exploration. Additional research in this area of display should prove quite beneficial. We are hopeful that future research will provide more detailed results.

5.3 Acknowledgements

The author is pleasure to acknowledge the technical support of ULVAC corporation and CPT corporation.

Reference

[1] E. Lawrence, and J. Tannas, Flat-Panel Displays and CRTs, Van Nostrand Reinhold (1995)

[2] G. Harbers, W. Timmers, and W. S. Smitt, *Proc. IDMC*, 313 (2002)

[3] J. A. Castellano, Hanbook of display technology, Chapter 8, Academic Press, Inc. (1992)

[4] R. Okoshi, *Proceeding of IEEE*, Vol. 68, 548 (1980)

[5] Y. Itoh, S. Fujiwara, N. Kimura, S. Mizuhima, F. Funada, and M. Hijikigawa, *Proc.SID*, Vol. 1,221 (1998)

[6] B. J. de Gans, P. C. Duineveld, and U. S. Schubert, *Adv. Mater.*, Vol. 16, 203-213 (2004)

[7] A. Asai, M. Dhioya, S. Hirasawa, and T. Okzaki, *AIChE J*. Vol. 41, 1357-1367 (1993)

[8] M. Ikegawa and H. Azuma, *JSME J., series B*, Vol. 47. 490-496 (2004)

[9] D. Pesach and A. Marmur, *Lungmuir*, Vol. 3, 519-524 (1987)

[10] J. Park and J. Moon, *Langmuir*, Vol. 22, 3506-3513 (2006)

[11] B.J. de Gans, *Langmuir*, Vol. 20, 789-7793 (2004)

[12] W. T. Pimbley, *IBM J. of Res. Dev*., Vol. 20, 148-156 (1977)

[13] D.M. Hartmann, O. Kibar, *Appl. Opt.*, Vol. 40, 2736-2746 (2001)

[14] M. Gindl, G. Sinn, W. Gindl, A. Reiterer, and S. Tschegg, *Colloids and Surfaces A*, Vol. 181,279-287 (2001).

[15] H. C. Jung, S. H. Cho, *Journ. of Electronic Mater.,* Vol. 36, 1211-1218 (2007)

[16] Richard L. Burden, J. Douglas Faires, Numerical Analysis, Brooks/Cole (2000)